Rapalogs downmodulate intrinsic immunity and promote cell entry of SARS-CoV-2

Guoli Shi[1], Abhilash I. Chiramel[2], Saliha Majdoul[1], Kin Kui Lai[1], Sudipto Das[3], Paul A. Beare[2], Thorkell Andresson[3], Sonja M. Best[2], Alex A. Compton[1,*]

[1]HIV Dynamics and Replication Program, Center for Cancer Research, National Cancer Institute, Frederick, MD 21702

[2]Laboratory of Virology, Rocky Mountain Laboratories, National Institute of Allergy and Infectious Diseases, Hamilton, MT 59840

[3]Protein Characterization Laboratory, Center for Cancer Research, National Cancer Institute, Frederick, MD 21702

[*]Address correspondence to alex.compton@nih.gov

Running title: Rapalogs promote cell entry of SARS-CoV-2

Keywords: rapamycin, rapalog, mTOR inhibitor, IFITM, interferon, SARS, COVID-19, coronavirus, Influenza, membrane fusion

Word count: 3,356 (Introduction, Results, and Discussion)

Abstract (246 words)

Infection by SARS-CoV-2 generally causes mild symptoms but can lead to severe disease and death in certain populations, including the immunocompromised. Drug repurposing efforts are underway to identify compounds that interfere with SARS-CoV-2 replication or the immunopathology it can elicit. Rapamycin is among those being currently tested in clinical trials for impacts on COVID-19 severity. While rapamycin and rapamycin analogs (rapalogs) are FDA-approved for use as mTOR inhibitors in multiple clinical settings, including cancer, we previously found that rapamycin can increase the susceptibility of cells to infection by Influenza A virus. In this study, we tested the impact of rapalogs on cellular susceptibility to SARS-CoV-2 infection. We report that rapamycin and rapalogs increased SARS-CoV-2 titers in human cervical epithelial and lung epithelial cell lines to different extents, and a similar pattern of enhancement was observed using pseudovirus incorporating viral fusion proteins from SARS-CoV-2, SARS-CoV, MERS, and Influenza A Virus. Rapalogs also promoted cell entry driven by SARS-CoV-2 Spike in nasal cells and primary small airway cells, representing proximal and distal ends of the human respiratory tract, respectively. Interestingly, cell entry enhancement by the rapalog ridaforolimus was cell type-dependent, revealing a previously unrecognized functional divergence between rapalogs. The differential activity of rapalogs was associated with their capacity to induce the degradation of interferon-inducible transmembrane (IFITM) proteins, restriction factors that broadly inhibit virus infection. Our findings will spur the development of mTOR inhibitors that do not suppress the cell's first line of antiviral defense.

Significance (120 words)

Due to a lack of effective antivirals available to combat SARS-CoV-2 infection and the disease it causes (COVID-19), existing drugs that are clinically-approved for use in humans are being considered for deployment during this protracted pandemic. Rapamycin is an immunosuppressant that is administered to humans suffering from cancer, autoimmunity, atherosclerosis, and organ transplant rejection. While generally recognized for its inhibitory effects on the adaptive immune response, we previously showed that rapamycin can also impair intrinsic immunity, the immune system present within all cells of the body. Here, we show that rapamycin and rapamycin analogs (rapalogs) promote the first step of the SARS-CoV-2 infection cycle—entry into cells—by inducing the destruction of antiviral proteins that stand guard during virus invasion.

Introduction

Severe acute respiratory syndrome (SARS) coronavirus (CoV)-2 emerged in humans in 2019 following a species jump from bats and a possible intermediate animal host and is the cause of COVID-19, a respiratory and multi-organ disease of variable severity [1, 2]. The characterization of virus-host interactions that dictate SARS-CoV-2 infection and COVID-19 severity is a major priority for public health [3]. Basic research aimed at identifying the cellular factors required for SARS-CoV-2 infection (host dependency factors) has provided targets for antiviral drug development or repurposing [4-10]. In parallel, the identification of cellular factors capable of inhibiting SARS-CoV-2 replication (host restriction factors) has revealed intrinsic antiviral defenses that should be maintained and bolstered in susceptible individuals, especially those immunocompromised by age, immunodeficiency, or medical regimen [11-13]. Immune

impairment, such as that resulting from cancer, has been associated with prolonged SARS-CoV-2 shedding and the seeding of "super-spreader" events [14-18]. As we consider host-directed small molecules as candidates for antiviral therapies, it remains critically important to assess their impact on both dependency factors and restriction factors before they are deployed to slow virus transmission and/or prevent viral pathogenesis in humans.

One group of compounds being considered for the prevention and treatment of COVID-19-related immunopathology are rapamycin (Rapamune, sirolimus) and rapamycin analogs (rapalogs) [19-30]. As Food and Drug Administration-approved inhibitors of mammalian target of rapamycin (mTOR) kinase, these drugs are used therapeutically as immunosuppressants to inhibit the processes of cancer, autoimmunity, graft versus host disease, atherosclerosis, and aging [31]. Rapalogs, including everolimus (RAD-001), temsirolimus (Torisel, CCI-779), and ridaforolimus (AP-23573), were developed to alter the bioavailability and half-life of rapamycin for improved pharmacodynamics *in vivo* [32-36]. Differing by only a single functional group appended to carbon-40 of rapamycin **(Figure 1)**, it is believed that rapamycin and rapalogs share the same molecular mechanism of action to inhibit mTOR [35]. Rapamycin binds to FK506-binding protein 12 (FKBP12) and the resulting complex physically interacts with mTOR and disrupts its signaling potential.

Activation of mTOR promotes cell growth, cell proliferation, and cell survival [37]. In addition, mTOR activation promotes pro-inflammatory T-cell differentiation and mTOR inhibitors have been used classically to block lymphocyte proliferation and cytokine storm [38]. Since respiratory virus infections can cause disease by provoking hyper-inflammatory immune responses that result in immunopathology, rapalogs are being tested as treatments to decrease viral disease burden. At least three active clinical trials have been designed to test the impact of rapamycin on COVID-19 severity (NCT04461340, NCT04341675, NCT04371640).

In addition to their potential utility for mitigating disease in individuals already infected by SARS-CoV-2, there are also calls to explore the use of rapalogs as antiviral agents to prevent infection itself [39]. It was previously reported that mTOR activation promotes infection by the human coronavirus that causes Middle East Respiratory Syndrome (MERS-CoV) [40]. However, the relationship between mTOR and virus replication is complex, varies from virus to virus, and is dynamic according to a given step in the virus life cycle [41-43].

Rapamycin and temsirolimus have been shown to promote Influenza A replication in mice and to exacerbate viral disease [44, 45]. Furthermore, we recently demonstrated that acute rapamycin treatment increases cellular susceptibility Influenza A virus infection by inducing the selective degradation of interferon-inducible transmembrane (IFITM) proteins [46]. IFITM proteins are expressed basally in a variety of tissues and are important components of cell-intrinsic immunity, the antiviral network that defends individual cells against virus invasion [47, 48]. We showed that rapamycin triggers the sorting of endosomal IFITM2 and IFITM3 into lysosomes for proteolytic degradation through a process that was independent of macroautophagy yet dependent on ubiquitin and endosomal complexes required for transport (ESCRT) machinery [46]. These findings revealed a previously unrecognized immunosuppressive feature of rapamycin acting on intrinsic immunity. Since IFITM proteins broadly inhibit the cellular entry of diverse enveloped viruses by disfavoring virus-cell membrane fusion in endosomes and at the plasma membrane [49-54], rapamycin exposure may increase cellular susceptibility to infection by many viral pathogens. We and others have previously shown that SARS-CoV-2 infection can be inhibited by ectopic and endogenous IFITM1, IFITM2, and/or IFITM3 in cell types that are permissive to infection [11, 13, 55, 56]. Additionally, single nucleotide polymorphisms in *IFITM3* known as ns12252 and

139 rs34481144, previously associated with severe outcomes in Influenza A infection, have been
140 associated with severe COVID-19 [57, 58]. Therefore, we tested the impact of rapamycin and
141 rapalogs (hereby collectively referred to as rapalogs) on SARS-CoV-2 infection and characterized
142 the stages of infection affected.
143
144 **Results**
145
146 Two cell lines, cervical epithelial cells transduced with human ACE2 and TMPRSS2
147 (HeLa-ACE2-TMPRSS2) and lung epithelial cells transduced with human ACE2 (A549-ACE2),
148 were pretreated with everolimus at varying concentrations for four hours prior to addition of
149 SARS-CoV-2. Cell culture media was harvested 24 hours after virus addition and infectious virus
150 titers were measured on Vero cells by plaque assay. We found that everolimus enhanced virus
151 titers in a dose dependent manner, with a 20 micromolar dose increasing infectious yields by 8-
152 fold in HeLa-ACE2-TMPRSS2 **(Figure 2A)** and by 3.5-fold in A549-ACE2 **(Figure 2B)**. The
153 effect of everolimus relative to other rapalogs was assessed by pretreating cells with 20 micromolar
154 amounts for four hours followed by addition of SARS-CoV-2. In HeLa-ACE2-TMPRSS2 cells,
155 rapamycin and temsirolimus promoted infection to a similar extent as everolimus, while the effect
156 of ridaforolimus was negligible **(Figure 2C)**. In A549-ACE2 cells, rapamycin and temsirolimus
157 enhanced infectious yield by 9- and 15-fold, respectively, while everolimus and ridaforolimus did
158 so to a smaller degree **(Figure 2D)**. There results indicate that rapalogs generally increase the
159 infectious yield of SARS-CoV-2 from cells.
160 To identify the stage of virus replication that is promoted by rapalogs, we took advantage
161 of a pseudovirus system based on human immunodeficiency virus. This pseudovirus (HIV-CoV-2
162 S) is limited to a single round of infection, cell entry is mediated by SARS-CoV-2 Spike, and
163 infection of target cells is measured by luciferase activity. Rapalogs were tested for activity on
164 HIV-CoV-2 S in HeLa-ACE2 cells, since, in contrast to SARS-CoV-2, this pseudovirus does not
165 require TMPRSS2 for cell entry. Rapamycin, everolimus, and temsirolimus enhanced HIV-CoV-
166 2 S infection by up to an order to magnitude, while ridaforolimus had little effect **(Figure 3A)**.
167 These results approximate those obtained using replication-competent SARS-CoV-2, revealing
168 that rapalogs promote the Spike-mediated cell entry step in a drug-dependent manner. We also
169 tested the effect of tacrolimus (FK506), a compound with a chemical structure nearly identical to
170 that of the rapalogs but which does not bind mTOR. We found that tacrolimus did not promote
171 infection of HeLa-ACE2 by HIV-CoV-2 S **(Supplemental Figure 1A)**.
172 Virus entry into cells is a concerted process involving virus attachment to the cell surface
173 followed by fusion of cellular and viral membranes. Therefore, we carried out a virus-cell fusion
174 assay in order to quantify the terminal stage of virus entry into single cells using flow cytometry.
175 We found that treatment of cells with rapamycin, everolimus, and temsirolimus resulted in
176 enhanced virus-cell fusion while ridaforolimus had no such effect **(Figure 3B and 3C)**. These
177 findings suggest that rapalogs promote the cell entry process mediated by SARS-CoV-2 Spike by
178 facilitating virus-cell membrane merger. To measure whether rapalogs promote the cell entry
179 process driven by other coronavirus Spike proteins, we produced HIV incorporating Spike from
180 SARS-CoV (HIV-CoV S) or MERS (HIV-MERS S). Infections by both HIV-CoV S and HIV-
181 MERS S were elevated by rapalog treatment of HeLa-ACE2 and HeLa-DPP4, respectively,
182 although the extent of enhancement was lower than that observed with HIV-CoV-2 S **(Figure 3D**
183 **and 3E)**. Consistently, ridaforolimus was the least active among the rapalogs tested and it did not
184 significantly promote pseudovirus infection. Since we previously showed that rapamycin promotes

185 the cell entry process of Influenza A virus, we also assessed infection of pseudovirus incorporating
186 hemagglutinin (HIV-HA). HA-mediated infection was enhanced 10-fold by rapamycin and
187 everolimus, while temsirolimus enhanced by more than 30-fold. In contrast, ridaforolimus was
188 inactive **(Supplemental Figure 1B)**.
189 SARS-CoV-2 can enter cells via multiple routes, and sequential proteolytic processing of
190 Spike is essential to this process. SARS-CoV-2 Spike is cleaved at a polybasic motif (RRAR)
191 located at the S1/S2 boundary by furin-like proteases in virus-producing cells prior to release.
192 Subsequently, the S2' site is cleaved by trypsin-like proteases such as TMPRSS2 on the target cell
193 surface or cathepsins B and L in target cell endosomes, activating the viral fusion peptide and
194 facilitating membrane fusion [59-61]. It was previously shown that deletion or mutation of the
195 polybasic RRAR motif in Spike promotes the endocytic, cathepsin-dependent entry pathway [4,
196 56], as has been shown for MERS Spike [62]. We found that inhibition of cathepsin activity by
197 E64d blocked pseudovirus infection in HeLa-ACE2 cells, while inhibition of TMPRSS2 activity
198 by camostat mesylate had little to no effect **(Figure 4A)**, supporting the notion that an endosomal
199 entry pathway is predominantly used by SARS-CoV-2 Spike in these cells [63]. To directly test
200 whether rapalogs enhance Spike-mediated entry at the plasma membrane or in endosomes, we
201 produced pseudovirus with Spike mutated at the polybasic $_{682}$RRAR$_{685}$ motif (RRAR → YSAS).
202 We confirmed that introduction of YSAS prevented cleavage of Spike into S1 and S2 subunits in
203 virus-producing cells **(Supplemental Figure 2)**. Using pseudovirus incorporating mutant spike,
204 we found that the capacity for select rapalogs to promote infection was mostly intact **(Figure 4B)**.
205 These results suggest that rapalog treatment facilitates endosomal Spike-mediated entry in HeLa-
206 ACE2 cells.
207 We previously demonstrated that mTOR inhibition by rapamycin triggers a rapid
208 degradation of IFITM proteins in various cell types, including HeLa, primary human foreskin
209 fibroblasts, and CD34+ hematopoietic stem cells [46]. To compare and contrast the effects of
210 rapalogs on steady-state IFITM protein levels, we treated HeLa-ACE2 cells with rapamycin,
211 everolimus, temsirolimus, or ridaforolimus for four hours. We found that everolimus and
212 temsirolimus treatment reduced levels of IFITM1, IFITM2, and IFITM3 proteins to a similar
213 extent as rapamycin, while ACE2 levels were unaffected. However, ridaforolimus resulted in only
214 a modest reduction of IFITM proteins **(Figure 5A)**. Rapalogs promote the proteolytic degradation
215 of IFITM proteins in endolysosomes, since this process was inhibited by bafilomycin A1
216 **(Supplemental Figure 3)**. To formally address how rapalog-mediated depletion of IFITM proteins
217 impacts SARS-CoV-2 Spike-mediated entry, we used HeLa cells in which IFITM1, IFITM2, and
218 IFITM3 are knocked out (*IFITM1-3* KO) and introduced human ACE2 by transient transfection
219 **(Figure 5B)**. Relative to WT cells, where temsirolimus promotes infection by approximately 10-
220 fold, the enhancement effect was reduced to 1.5-fold in *IFITM1-3* KO cells. Furthermore,
221 pseudovirus infection was approximately 50-fold higher in *IFITM1-3* KO cells. These findings
222 indicate that endogenous IFITM1, IFITM2, and IFITM3 substantially restrict SARS-CoV-2 Spike-
223 mediated infection in HeLa-ACE2 cells and that rapalogs promote infection by lowering their
224 levels in cells. In order to better characterize the degradation program triggered by rapalogs and to
225 identify cellular proteins other than IFITM that are modulated following rapalog treatment, we
226 performed proteomics by mass spectrometry on HeLa-ACE2 cells treated with DMSO,
227 temsirolimus, or ridaforolimus. The complete list of over 7000 proteins detected is available in
228 **Supplemental File 1**. While the IFITM proteins themselves were not detected in our analysis, we
229 identified a select number of additional proteins whose levels were decreased significantly by
230 rapamycin and/or temsirolimus and, to a lesser extent, by ridaforolimus **(Supplemental Figure 4)**.

To explore the impact of rapalogs on SARS-CoV-2 infection in additional cell types that model the human respiratory tract, we used primary human small airway (lung) epithelial cells (herein referred to as small airway cells) and partially transformed human nasal epithelial cells (UNCNN2TS, herein referred to as nasal cells) [64, 65]. These cells were not permissive to HIV-CoV-2 S pseudovirus, but we were able to infect them with a pseudovirus based on vesicular stomatitis virus (VSV-CoV-2 S) [66]. We found that small airway cells were highly permissive to VSV-CoV-2 S and that rapalogs promoted infection to different extents. Specifically, rapamycin, everolimus, and temsirolimus enhanced infection by up to 2.5-fold while ridaforolimus was less active **(Figure 6A)**. In order to draw parallels between the mechanism of action of rapalogs on different cell types, we assessed the basal levels of IFITM proteins in small airway cells and tested whether their levels were altered by the drugs. Endogenous IFITM3 protein was detected and was reduced to different extents by rapalogs, while IFITM1 was found at lower levels and IFITM2 was not detected at all **(Figure 6B)**. We then asked whether IFITM3 in small airway cells was consequential for VSV-CoV-2 S infection by using RNA interference. Interestingly, transfection of control siRNA resulted in increased IFITM1 protein relative to basal levels, but not that of IFITM2, and specific knockdown of IFITM3 resulted in a more than 3-fold enhancement of infection **(Figure 6C)**. These results suggest that rapalogs promote SARS-CoV-2 Spike-mediated infection in small airway cells, at least in part, by downmodulating IFITM3. We performed a similar series of experiments in nasal cells and found that, while these cells were relatively resistant to VSV-CoV-2 S pseudovirus, infection levels were elevated in the presence of rapalogs **(Figure 6D)**. Here, rapamycin, everolimus, and ridaforolimus treatment resulted in higher levels of infection compared to temsirolimus treatment, indicating that the bioactivity of some rapalogs is cell-type dependent. When we examined the extent to which endogenous IFITM proteins were modulated by the drugs in nasal cells, we found that IFITM3 was abundantly expressed and was differentially downmodulated by rapalogs, with temsirolimus exhibiting the lowest capacity to decrease IFITM3 levels. In these cells, IFITM1 was barely detectable and IFITM2 was not detected **(Figure 6E)**. As seen in small airway cells, siRNA transfection induced IFITM1 protein in nasal cells. Upon specific knockdown of IFITM3, infection was enhanced by more than 20-fold **(Figure 6F)**. Overall, these data support a model whereby rapalog treatment of cells modeling the human respiratory tract results in drug-dependent degradation of IFITM proteins and increased susceptibility to SARS-CoV-2 Spike-mediated infection.

Discussion

We previously demonstrated that treatment of cells with micromolar quantities of rapamycin induces the lysosomal degradation of IFITM proteins via a pathway that is independent of macroautophagy but dependent upon ESCRT-mediated sorting of IFITM proteins into intraluminal vesicles of late endosomes [46]. Our understanding of how this degradation pathway is mediated is incomplete, but it likely results from a form of non-canonical autophagy known as microautophagy [67]. One type of microautophagy that has been described in yeast and mammalian cells is characterized by ESCRT-dependent sorting of endolysosomal membrane proteins into intraluminal vesicles followed by their degradation by lysosomal hydrolases. Furthermore, there is evidence indicating that microautophagy is regulated by mTOR [68]. It was recently shown in yeast that mTOR inhibition triggers a ubiquitin- and ESCRT-dependent turnover of vacuolar (lysosomal) membrane proteins [69, 70]. Apart from our immunoblotting of IFITM proteins, our proteomics analysis suggests that rapalogs differentially induce a program that turns

277 over a select group of cellular proteins (1% or less of proteins detected were reduced by 40% or
278 more following treatment with any rapalog). Ongoing work will identify whether these proteins
279 are co-regulated directly or indirectly by the same E3 ubiquitin ligase, and whether this ligase is
280 controlled by mTOR activity.

281 IFITM2 and IFITM3 are cell surface proteins which are targeted to endolysosomes via a
282 tyrosine-based endocytic motif (YxxL) in the amino terminus, and phosphorylation regulates this
283 process [71-75]. In contrast, it is often cited that IFITM1, which lacks the YxxL motif, is primarily
284 localized to the plasma membrane of cells. However, the carboxy-terminus of IFITM1 contains its
285 own sorting signal and is responsible for a proportion of IFITM1 being localized to endosomes
286 [76, 77]. Our previous efforts found that FLAG-tagged IFITM2 and IFITM3 were sensitive to
287 rapamycin-induced degradation while FLAG-IFITM1 was not [46]. In the current study, we find
288 that all three of the IFITM proteins, which are expressed at high basal levels in HeLa cells, are
289 degraded following rapalog treatment. This likely reflects a partial overlap in endolysosomal
290 localization between IFITM1, IFITM2, and IFITM3. In support of IFITM1 being partially
291 localized to lysosomes is the fact that it inhibits the cell entry of Marburg and Ebola viruses, which
292 require lysosomal cathepsins for the final step of viral fusion [78]. There remains much to be
293 learned about the sequence determinants and cellular machinery required to carry out degradation
294 of IFITM proteins during rapalog treatment. It was previously discovered that NEDD4 E3 ligase
295 regulates the degradation of IFITM2 and IFITM3 [74, 79], but whether other E3 ligases mediate
296 the regulation of IFITM proteins during mTOR inhibition is unknown.

297 In addition to the degradation of basal IFITM3 expressed at steady-state, we previously
298 reported that rapamycin promotes the turnover of IFITM3 induced by type-I interferon [46]. While
299 our results indicate that rapalogs differentially impact basal levels of IFITM proteins in multiple
300 cell types, we did not assess how they affect those induced by infection. This would be required to
301 fully understand how rapalogs promote cellular susceptibility to infection, and to what extent
302 rapalog-mediated regulation of IFITM proteins is responsible. In contrast to HeLa cells, we did
303 not detect IFITM1, IFITM2, or IFITM3 protein in A549 cells under basal conditions. Nonetheless,
304 it has been shown that IFITM3 is among the most highly induced genes in primary human lung
305 epithelial cells exposed to SARS-CoV-2 [82, 83]. Therefore, it is possible that cell type-specific
306 patterns of virus-induced IFITM will need to be assessed in order to fully understand the effects
307 of different rapalogs on cellular susceptibility to virus infection. Nonetheless, it is notable that we
308 observed a relatively high level of basal IFITM3 present in nasal epithelial cells, and furthermore,
309 that specific knockdown of IFITM3 resulted in a more than 20-fold gain in cellular susceptibility
310 to SARS-CoV-2 Spike-mediated infection in this cell type. The upper airway, and the nasal
311 epithelium in particular, likely represents the initial site of infection by SARS-CoV-2 [84]. It was
312 reported that infected humans experiencing mild or moderative COVID-19 showed extensive
313 induction of antiviral genes, including *IFITM1* and *IFITM3*, in their nasal epithelium compared to
314 individuals suffering from more severe COVID-19 [85]. This finding suggests that cell-intrinsic
315 immunity in the nasal epithelium plays a role in constraining virus-induced pathology in the lower
316 respiratory tract. Taken together, these results suggest that rapalog use and its downmodulating
317 effects on IFITM proteins may facilitate virus spread between humans. It would be interesting to
318 examine whether any of the other proteins differentially downmodulated or upmodulated by
319 rapalogs have an impact on SARS-CoV-2 infection in the various cell types studied here.

320 All of the rapamycin-derived compounds tested here are believed to act as allosteric mTOR
321 inhibitors by promoting a tertiary complex consisting of drug, FKBP12, and mTOR. In contrast,
322 tacrolimus (FK506) binds FKBP12 and calcineurin, but not mTOR [80]. The fact that tacrolimus

323 does not enhance SARS-CoV-2 Spike-mediated infection suggests that mTOR inhibition is
324 essential to this process. However, we also show that ridaforolimus enhances virus infection in
325 HeLa and A549 cells to a lesser extent than the other rapalogs, which suggests that binding to
326 mTOR and FKBP12 is insufficient to explain the phenotype. It is possible that enhancement of
327 infection results from interactions between rapalogs and cellular proteins other than mTOR and
328 FKBP12. Rapamycin has been shown to bind additional FKBPs, such as FKBP52, whose levels
329 may vary between cell types [81]. Our results warrant an in-depth analysis of the cellular proteins
330 directly bound by different rapalogs, and this should be carried out in different cell lines, since we
331 show that the impact of ridaforolimus on infection is cell-type dependent.
332 Overall, and in combination with our previous work [46], these results draw attention to a
333 novel immunosuppressive property of rapamycin and rapalogs that acts on intrinsic immunity and
334 impacts cellular susceptibility to infection by multiple viruses, including SARS-CoV-2. Rapalogs
335 are traditionally used for their immunosuppressive effects on adaptive immunity in order to
336 mitigate systemic immunopathology, and this is one reason why they are being tested for
337 therapeutic benefit in COVID-19 patients suffering from respiratory distress syndrome. Further
338 work exploring how dosing of existing rapalogs in animal models impacts both the intended and
339 unintended consequences of mTOR inhibition is a priority. Furthermore, the development of new
340 mTOR inhibitors lacking this effect on intrinsic immunity are needed in order to minimize
341 unintended immunocompromised states in humans.
342
343 **Materials and Methods**
344
345 **Cell lines, cell culture, and inhibitors**
346
347 HEK293T cells were obtained from ATCC (CRL-3216). HeLa-ACE2, HeLa-ACE2-TMPRSS2,
348 HeLa-DPP4, and A549-ACE2 cell lines were produced by transducing cells with lentivirus
349 packaging pWPI encoding ACE2, DPP4, or TMPRSS2 and selecting with blasticidin. HeLa
350 IFITM1/2/3 Knockout (C5-9) cells were purchased from ATCC (CRL-3452). Primary human
351 small airway (lung) epithelial cells (HSAEC) were purchased from ATCC (PCS-301-010). The
352 partially-immortalized nasal epithelial cell line (UNCNN2TS) was kindly provided by Scott H.
353 Randell (University of North Carolina School of Medicine). All cells were cultured at 37°C with
354 5% CO_2 in Dulbecco's Modified Eagle Medium (DMEM) supplemented with 10% fetal bovine
355 serum (HyClone, Cytiva), except for UNCNN2TS, which were cultured in EpiX Medium
356 (Propagenix), and HSAEC, which were cultured with airway epithelial cell basal medium (ATCC,
357 PCS-300-030) and the bronchial epithelial cell growth kit (ATCC, PCS-300-040). Rapamycin
358 (553211) was obtained from Sigma. Everolimus (S1120), temsirolimus (S1044), ridaforolimus
359 (S5003), and tacrolimus (S5003) were obtained from Selleckchem. E64d (E8640) and camostat
360 mesylate (SML0057) were obtained from Sigma.
361
362 **Plasmids and RNA interference**
363
364 pcDNA3.1 encoding human ACE2 was kindly provided by Thomas Gallagher (Loyola
365 University). pcDNA3.1 encoding CoV Spike or CoV-2 Spike tagged with a C9 epitope on the C-
366 terminus, or MERS Spike, were kindly provided by Thomas Gallagher (Loyola University).
367 pcDNA3.1 CoV-2 Spike encoding YSAS in the place of $_{682}$RRAR$_{685}$ was generated by site-
368 directed mutagenesis. pcDNA3.1 encoding CoV Spike or CoV-2 Spike tagged with a FLAG

369 epitope on the C-terminus, or VSV glycoprotein (VSV-G), were obtained from Michael Letko and
370 Vincent Munster (NIAID). pWPI was obtained from Addgene (12254) and human ACE2 or human
371 TMPRSS2 was introduced by Gateway cloning (Gateway LR Clonase II Enzyme mix (11791020))
372 as per manufacturer's instructions. pPolII encoding hemagglutinin (HA) or neuraminidase (NA)
373 from Influenza A/Turkey/1/2005 (H5N1) were kindly provided by Richard Yi Tsun Kao (The
374 University of Hong Kong). pCMV encoding HIV-1 Vpr fused to beta lactamase (pCMV4-BlaM-
375 Vpr) was obtained from ATCC (21950). pNL4-3LucR-E- was kindly provided by Vineet
376 KewalRamani. pNL4-3E- was kindly provided by Olivier Schwartz (Institut Pasteur). Silence
377 Select siRNA targeting IFITM3 (s195035) and a non-targeting control (No. 1) were obtained from
378 Ambion. Cells were transfected with 20 nM siRNA using Opti-MEM (Gibco) and Lipofectamine
379 RNAiMAX (Thermo Fisher).
380
381 **Virus and pseudovirus infections**
382
383 SARS-CoV-2 strain nCoV-WA1-2020 (MN985325.1) was provided by the Centers for Disease
384 Control. Virus propagation was performed in Vero E6 cells. Virus titers were calculated by plaque
385 assay performed in Vero E6 cells as follows: Serial 10-fold dilutions were added to Vero E6
386 monolayers in 48-well plates for 1 hour at 37°C. Cells were overlayed with 1.5% carboxymethyl
387 cellulose (Sigma) in modified Eagle's medium containing 3% fetal bovine serum (Gibco), 1 mM
388 L-glutamine, 50 units per mL penicillin and 50 µg per mL streptomycin. Three days post-infection,
389 cells were fixed in 10% formalin and stained with crystal violet to visualize and count plaques as
390 previously described [86]. Titers were calculated as plaque forming units per mL and normalized
391 as described in the figure captions. HIV-based pseudovirus was produced by transfecting
392 HEK293T cells with 12 µg of pNL4-3LucR-E- and 4 µg of pcDNA3.1 Spike (CoV, CoV-2, or
393 MERS), or 2 µg of pPol1II HA and 2 µg of pPol1II NA using TransIT-293 (Mirus). Virus
394 supernatant was harvested 72 hours post-transfection and filtered through 0.22 µm filters.
395 Undiluted virus supernatant was added to target cells and incubated for 72 hours prior to lysis with
396 Passive Lysis Buffer (Promega). Luciferase activity was measured using the Luciferase Assay
397 System (Promega). VSV-based pseudovirus was produced as previously described [66]. In brief,
398 HEK293T cells were transfected with 2 µg pcDNA3.1 and CoV, CoV-2, or MERS Spike using
399 Lipofectamine2000 (Thermo Fisher). At 24 hours post-transfection, culture medium was removed
400 from cells and 2 mL of VSV-luc/GFP + VSV-G was added. At 48 hours post-infection, virus
401 supernatants were collected, clarified by centrifugation at 500xG for 5 mins, and stored. 50-200
402 µL of virus supernatants were added to target cells for a period of 24 hours prior to fixation with
403 4% paraformaldehyde (for measurements of GFP+ cells with flow cytometry) or lysis with Passive
404 Lysis Buffer (for measurements of luciferase activity). E64d or camostat mesylate (25 µM) were
405 used to pretreat cells for 2 hours prior to virus addition and were maintained for the duration of
406 infection. For infections with replication-competent SARS-CoV-2, rapamycin, everolimus,
407 temsirolimus, or ridaforolimus (20 µM) were used to pretreat cells for 4 hours and then drugs were
408 washed away prior to addition of virus at a multiplicity of infection (MOI) of 0.1. DMSO (Sigma)
409 was used as a vehicle control. At 1 hour post-virus addition, cells were washed once with 1X PBS
410 and overlayed with complete medium. Supernatants were harvested 24 hours later and titers were
411 determined on plaque assays performed in Vero E6 cells. For single-round infections using HIV-
412 or VSV-based pseudovirus, rapamycin, everolimus, temsirolimus, ridaforolimus, or tacrolimus (20
413 µM) were used to pretreat cells for 4 hours and were maintained for the duration of infection and

414 until harvest of cells for luciferase assay or flow cytometry. DMSO (Sigma) was used as a vehicle
415 control.
416
417 **FRET-based virus-cell fusion assay**
418
419 HIV-based pseudovirus incorporating BlaM-Vpr and CoV-2 Spike was produced by transfecting
420 HEK293T cells with pNL4-3E- (15 µg), pCMV4-BlaM-Vpr (5 µg), and pcDNA3.1 CoV-2 Spike
421 (5 µg) using the calcium phosphate technique. Briefly, six million 293T cells were seeded in a T75
422 flask. Plasmid DNA was mixed with sterile H_2O, $CaCl_2$, and Tris-EDTA (TE) buffer, and the
423 totality was combined with Hepes-buffered saline (HBS). The transfection volume was added
424 dropwise, and cells were incubated at 37°C for 48 h. Supernatants were clarified by centrifugation,
425 passed through a 0.45 µm filter, and stored. Titers were measured using an HIV-1 p24 ELISA kit
426 (XpressBio). 50 ng p25 equivalent of virus was added to HeLa-ACE2 cells for 2 hours. Cells were
427 washed and labeled with the CCF2-AM β-lactamase Loading Kit (Invitrogen) for 2 hours and
428 analyzed for virus-cell fusion by flow cytometry as described [87]. Rapamycin, everolimus,
429 temsirolimus, or ridaforolimus (20 µM) were used to pretreat cells for 4 hours prior to virus
430 addition and were maintained for the duration of infection. DMSO (Sigma) was used as a vehicle
431 control.
432
433 **Western blot, flow cytometry, and antibodies**

434 Whole cell lysis was performed with RIPA buffer (Thermo Fisher) supplemented with Halt
435 Protease Inhibitor mixture EDTA-free (Thermo Fisher). Lysates were clarified by centrifugation
436 and supernatants were collected and stored. Protein concentration was determined with the Protein
437 Assay Kit II (Bio-Rad), and 10-15 µg of protein was loaded into 12% acrylamide Criterion XT
438 Bis-Tris Precast Gels (Bio-Rad). Electrophoresis was performed with NuPage MES SDS Running
439 Buffer (Invitrogren) and proteins were transferred to Amersham Protran Premium Nitrocellulose
440 Membrane, pore size 0.20 µm (GE Healthcare). Membranes were blocked with Odyssey Blocking
441 Buffer in PBS (Li-COR) and incubated with the following primary antibodies diluted in Odyssey
442 Antibody Diluent (Li-COR): anti-IFITM1 (60074-1-Ig; Proteintech), anti-IFITM2 (66137-1-Ig;
443 Proteintech), anti-IFITM3 (EPR5242, ab109429; Abcam), anti-actin (C4, sc-47778; Santa Cruz
444 Biotechnology), anti-hACE2 (ab15348; Abcam), and anti-CoV Spike (PA1-41165; Thermo
445 Fisher). Secondary antibodies conjugated to DyLight 800 or 680 (Li-Cor) and the Li-Cor Odyssey
446 CLx imaging system were used to reveal specific protein detection. Images were analyzed and
447 assembled using ImageStudioLite (Li-Cor).
448
449 **Proteomics by mass spectrometry**
450
451 <u>Protein Digestion and TMT labeling.</u> Cell pellets were produced in triplicate from HeLa-ACE2
452 cells treated with 20 µM rapamycin, temsirolimus, ridaforolimus, or an equivalent volume of
453 DMSO and lysed in 50 mM HEPES, pH 8.0 and 8M urea followed by sonication. Lysates were
454 clarified by centrifugation and protein concentration was quantified using BCA protein estimation
455 kit (Thermo Fisher). One hundred micrograms of lysate were alkylated and digested by addition
456 of trypsin at a ratio of 1:50 (Promega) and incubating overnight at 37ºC. Digestion was acidified
457 by adding formic acid (FA) to a final concentration of 1% and desalted using peptide desalting
458 columns (Thermo Fisher) according to manufacturer's protocol. Peptides were eluted from the

459 columns using 50% ACN/0.1% FA, dried in a speedvac, and kept frozen at -20ºC until further
460 analysis. For TMT labeling, 15 µg of each sample was reconstituted in 50 µL of 50 mM HEPES,
461 pH 8.0, and 75 µg of TMTpro label (Thermo Fisher) in 100% ACN was added to each sample.
462 After incubating the mixture for 1 hr at room temperature with occasional mixing, the reaction was
463 terminated by adding 8 µL of 5% hydroxylamine. The peptide samples for each condition were
464 pooled and cleaned using peptide desalting columns (Thermo Fisher). High pH reverse phase
465 fractionation. The first dimensional separation of the peptides was performed using a Waters
466 Acquity UPLC system coupled with a fluorescence detector (Waters) using a 150 mm x 3.0 mm
467 Xbridge Peptide BEM™ 2.5 um C18 column (Waters) operating at 0.35 mL/min. The dried
468 peptides were reconstituted in 100 µL of mobile phase A solvent (3 mM ammonium bicarbonate,
469 pH 8.0). Mobile phase B was 100% acetonitrile (Thermo Fisher). The column was washed with
470 mobile phase A for 10 min followed by gradient elution 0- 50% B (10-60 min) and 50-75 %B (60-
471 70 min). The fractions were collected every minute. These 60 fractions were pooled into 24
472 fractions. The fractions were vacuum centrifuged to dryness and stored at -80ºC until analysis by
473 mass spectrometry. Mass Spectrometry acquisition and data analysis. The dried peptide fractions
474 were reconstituted in 0.1% TFA and subjected to nanoflow liquid chromatography (Thermo
475 Ultimate™ 3000RSLC nano LC system, Thermo Scientific) coupled to an Orbitrap Eclipse mass
476 spectrometer (Thermo Scientific). Peptides were separated using a low pH gradient using 5-50%
477 ACN over 120 minutes in mobile phase containing 0.1% formic acid at 300 nL/min flow rate. MS
478 scans were performed in the Orbitrap analyser at a resolution of 120,000 with an ion accumulation
479 target set at $4e^5$ and max IT set at 50ms over a mass range of 400-1600 m/z. Ions with determined
480 charge states between 2 and 5 were selected for MS2 scans in the ion trap with CID fragmentation
481 (Turbo; NCE 35%; maximum injection time 35 ms; AGC 1×10^4). The spectra were searched
482 using the Real Time Search Node in the tune file using human Uniprot database using Comet
483 search algorithm with TMT16 plex (304.2071Da) set as a static modification of lysine and the N-
484 termini of the peptide. Carbamidomethylation of cysteine residues (+57.0214 Da) was set as a
485 static modification, while oxidation of methionine residues (+15.9949 Da) was set up as dynamic
486 modification. For the selected peptide, an SPS–MS3 scan was performed using up to 10 *b*- and *y*-
487 type fragment ions as precursors in an Orbitrap at 50,000 resolution with a normalized AGC set at
488 500 followed by maximum injection time set as "Auto" with a normalized collision energy setting
489 of 65. Acquired MS/MS spectra were searched against a human Uniprot protein database along
490 with a contaminant protein database, using a SEQUEST and percolator validator algorithms in the
491 Proteome Discoverer 2.4 software (Thermo Scientific). The precursor ion tolerance was set at 10
492 ppm and the fragment ions tolerance was set at 0.02 Da along with methionine oxidation included
493 as dynamic modification. Carbamidomethylation of cysteine residues and TMT16 plex
494 (304.2071Da) was set as a static modification of lysine and the N-termini of the peptide. Trypsin
495 was specified as the proteolytic enzyme, with up to 2 missed cleavage sites allowed. Searches used
496 a reverse sequence decoy strategy to control for the false peptide discovery and identifications
497 were validated using percolator software. Reporter ion intensities were adjusted to correct for the
498 impurities according to the manufacturer's specification and the abundances of the proteins were
499 quantified using the summation of the reporter ions for all identified peptides. The reporter
500 abundances were normalized across all the channels to account for equal peptide loading. Data
501 from the first replicate of the DMSO, rapamycin, and temsirolimus conditions was excluded from
502 the analysis due to their being identified as outliers in Principal Component Analysis. As such,
503 mean abundance values for DMSO, rapamycin, and temsirolimus were calculated from two
504 replicates while mean abundance values for ridaforolimus was calculated from three replicates.

Acknowledgements

We thank Scott H. Randell for providing the UNCNN2TS nasal epithelial cell line, Michael Letko and Vincent Munster for providing VSV-luc/GFP seed particles and CoV and CoV-2 Spike plasmids, Thomas Gallagher for providing CoV, CoV-2, and MERS Spike plasmids, and Eric Freed for providing primary human small airway epithelial cells.

Funding sources

Work in the lab of AAC was funded by the Intramural Research Program, National Institutes of Health, National Cancer Institute, Center for Cancer Research and an Intramural Targeted Anti-COVID-19 award from the National Institute of Allergy and Infectious Diseases. Work in the lab of SMB was funded by the Division of Intramural Research, National Institutes of Health, National Institute of Allergy and Infectious Diseases.

References

1. Zhu N, Zhang D, Wang W, Li X, Yang B, Song J, Zhao X, Huang B, Shi W, Lu R, et al: **A Novel Coronavirus from Patients with Pneumonia in China, 2019.** *New England Journal of Medicine* 2020, **382:**727-733.
2. Wu F, Zhao S, Bin Y, Chen Y-M, Wang W, Song Z-G, Hu Y, Tao Z-W, Tian J-H, Pei Y-Y, et al: **A new coronavirus associated with human respiratory disease in China.** *Nature* 2020**:**1-20.
3. Zhang X, Tan Y, Ling Y, Lu G, Liu F, Yi Z, Jia X, Wu M, Shi B, Xu S, et al: **Viral and host factors related to the clinical outcome of COVID-19.** *Nature* 2020**:**1-18.
4. Zhu Y, Feng F, Hu G, Wang Y, Yu Y, Zhu Y, Cai X, Sun Z, Han W, Ye R, et al: **A genome-wide CRISPR screen identifies host factors that regulate SARS-CoV-2 entry.** *Nature Communications* 2021**:**1-11.
5. Heaton BE, Trimarco JD, Hamele CE, Harding AT, Tata A, Zhu X, Tata PR, Smith CM, Heaton NS: **SRSF protein kinases 1 and 2 are essential host factors for human coronaviruses including SARS-CoV-2.** *bioRxiv* 2020**:**2020.2008.2014.251207.
6. Daniloski Z, Jordan TX, Wessels H-H, Hoagland DA, Kasela S, Legut M, Maniatis S, Mimitou EP, Lu L, Geller E, et al: **Identification of Required Host Factors for SARS-CoV-2 Infection in Human Cells.** *Cell* 2021, **184:**92-105.e116.
7. Wang R, Simoneau CR, Kulsuptrakul J, Bouhaddou M, Travisano KA, Hayashi JM, Carlson-Stevermer J, Zengel JR, Richards CM, Fozouni P, et al: **Genetic Screens Identify Host Factors for SARS- CoV-2 and Common Cold Coronaviruses.** *Cell* 2021, **184:**106-119.e114.
8. Hoffmann HH, Schneider WM, Rozen-Gagnon K, Miles LA, Schuster F, Razooky B, Jacobson E, Wu X, Yi S, Rudin CM, et al: **TMEM41B Is a Pan-flavivirus Host Factor.** *Cell* 2021, **184:**133-148.e120.
9. Schneider WM, Luna JM, Hoffmann HH, Sánchez-Rivera FJ, Leal AA, Ashbrook AW, Le Pen J, Ricardo-Lax I, Michailidis E, Peace A, et al: **Genome-Scale Identification of SARS-CoV-2 and Pan-coronavirus Host Factor Networks.** *Cell* 2021, **184:**120-132.e114.

550 10. Wei J, Alfajaro MM, DeWeirdt PC, Hanna RE, Lu-Culligan WJ, Cai WL, Strine MS,
551 Zhang S-M, Graziano VR, Schmitz CO, et al: **Genome-wide CRISPR Screens Reveal**
552 **Host Factors Critical for SARS-CoV-2 Infection.** *Cell* 2021, **184:**76-91.e13.
553 11. Zhao X, Zheng S, Chen D, Zheng M, Li X, Li G, Lin H, Chang J, Zeng H, Guo J-T: **LY6E**
554 **Restricts Entry of Human Coronaviruses, Including Currently Pandemic SARS-**
555 **CoV-2.** *Journal of Virology* 2020, **94**.
556 12. Martin-Sancho L, Lewinski MK, Pache L, Stoneham CA, Yin X, Pratt D, Churas C,
557 Rosenthal SB, Liu S, De Jesus PD, et al: **Functional Landscape of SARS-CoV-2 Cellular**
558 **Restriction.** *bioRxiv* 2020**:**2020.2009.2029.319566.
559 13. Zang R, Case JB, Yutuc E, Ma X, Shen S, Gomez Castro MF, Liu Z, Zeng Q, Zhao H, Son
560 J, et al: **Cholesterol 25-hydroxylase suppresses SARS-CoV-2 replication by blocking**
561 **membrane fusion.** *Proceedings of the National Academy of Sciences of the United States*
562 *of America* 2020, **32:**202012197.
563 14. Aydillo T, Babady NE, Kamboj M: **Shedding of Viable SARS-CoV-2 after**
564 **Immunosuppressive Therapy for Cancer.** *New England Journal of Medicine* 2020,
565 **383:**2586-2588.
566 15. Wei J, Zhao J, Han M, Meng F, Zhou J: **SARS-CoV-2 infection in immunocompromised**
567 **patients: humoral versus cell-mediated immunity.** *Journal for Immunotherapy of*
568 *Cancer* 2020, **8:**e000862.
569 16. Tarhini H, Recoing A, Bridier-Nahmias A, Rahi M, Lambert C, Martres P, Lucet J-C,
570 Rioux C, Bouzid D, Lebourgeois S, et al: **Long term SARS-CoV-2 infectiousness among**
571 **three immunocompromised patients: from prolonged viral shedding to SARS-CoV-2**
572 **superinfection.** *The Journal of Infectious Diseases* 2021.
573 17. Baang JH, Smith C, Mirabelli C, Valesano AL, Manthei DM, Bachman MA, Wobus CE,
574 Adams M, Washer L, Martin ET, Lauring AS: **Prolonged Severe Acute Respiratory**
575 **Syndrome Coronavirus 2 Replication in an Immunocompromised Patient.** *The*
576 *Journal of Infectious Diseases* 2021, **223:**23-27.
577 18. Avanzato VA, Matson MJ, Seifert SN, Pryce R, Williamson BN, Anzick SL, Barbian K,
578 Judson SD, Fischer ER, Martens C, et al: **Case Study: Prolonged Infectious SARS-CoV-**
579 **2 Shedding from an Asymptomatic Immunocompromised Individual with Cancer.**
580 *Cell* 2020, **183:**1901-1912.e1909.
581 19. Gordon DE, Jang GM, Bouhaddou M, Xu J, Obernier K, White KM, O'Meara MJ, Rezelj
582 VV, Guo JZ, Swaney DL, et al: **A SARS-CoV-2 protein interaction map reveals targets**
583 **for drug repurposing.** *Nature* 2020**:**1-30.
584 20. Zhou Y, Hou Y, Shen J, Huang Y, Martin W, Cheng F: **Network-based drug repurposing**
585 **for novel coronavirus 2019-nCoV/SARS-CoV-2.** *Cell Discovery* 2020**:**1-18.
586 21. Appelberg S, Gupta S, Svensson Akusjärvi S, Ambikan AT, Mikaeloff F, Saccon E,
587 Végvári Á, Benfeitas R, Sperk M, Ståhlberg M, et al: **Dysregulation in Akt/mTOR/HIF-**
588 **1 signaling identified by proteo-transcriptomics of SARS-CoV-2 infected cells.**
589 *Emerging Microbes & Infections* 2020, **9:**1748-1760.
590 22. Blagosklonny MV: **From causes of aging to death from COVID-19.** *Aging* 2020,
591 **12:**10004-10021.
592 23. Ciliberto G, Mancini R, Paggi MG: **Drug repurposing against COVID-19: focus on**
593 **anticancer agents.** *Journal of Experimental & Clinical Cancer Research* 2020, **39:**86.
594 24. Husain A, Byrareddy SN: **Rapamycin as a potential repurpose drug candidate for the**
595 **treatment of COVID-19.** *Chemico-Biological Interactions* 2020, **331:**109282.

596 25. Zheng Y, Li R, Liu S: **Immunoregulation with mTOR inhibitors to prevent COVID-**
597 **19 severity: A novel intervention strategy beyond vaccines and specific antiviral**
598 **medicines.** *Journal of Medical Virology* 2020, **92:**1495-1500.
599 26. Terrazzano G, Rubino V, Palatucci AT, Giovazzino A, Carriero F, Ruggiero G: **An Open**
600 **Question: Is It Rational to Inhibit the mTor-Dependent Pathway as COVID-19**
601 **Therapy?** *Frontiers in Pharmacology* 2020, **11:**856.
602 27. Ramaiah MJ: **mTOR inhibition and p53 activation, microRNAs: The possible therapy**
603 **against pandemic COVID-19.** *Gene Reports* 2020, **20:**100765.
604 28. Zhavoronkov A: **Geroprotective and senoremediative strategies to reduce the**
605 **comorbidity, infection rates, severity, and lethality in gerophilic and gerolavic**
606 **infections.** *Aging* 2020, **12:**6492-6510.
607 29. Willyard C: **Ageing and Covid Vaccines.** *Nature* 2020, **586:**352-354.
608 30. Omarjee L, Janin A, Perrot F, Laviolle B, Meilhac O, Mahe G: **Targeting T-cell**
609 **senescence and cytokine storm with rapamycin to prevent severe progression in**
610 **COVID-19.** *Clinical Immunology* 2020, **216:**108464.
611 31. Laplante M, Sabatini DM: **mTOR signaling in growth control and disease.** *Cell* 2012,
612 **149:**274-293.
613 32. Bertram PG, Zeng C, Thorson J, Shaw AS, Zheng XF: **The 14-3-3 proteins positively**
614 **regulate rapamycin-sensitive signaling.** *Current Biology* 1998, **8:**1259-1267.
615 33. Vignot S, Faivre S, Aguirre D, Raymond E: **mTOR-targeted therapy of cancer with**
616 **rapamycin derivatives.** *Annals of Oncology* 2005, **16:**525-537.
617 34. Lamming DW, Ye L, Sabatini DM, Baur JA: **Rapalogs and mTOR inhibitors as anti-**
618 **aging therapeutics.** *Journal of Clinical Investigation* 2013, **123:**980-989.
619 35. Abdel-Magid AF: **Rapalogs Potential as Practical Alternatives to Rapamycin.** *ACS*
620 *Medicinal Chemistry Letters* 2019, **10:**843-845.
621 36. Benjamin D, Colombi M, Moroni C, Hall MN: **Rapamycin passes the torch: a new**
622 **generation of mTOR inhibitors.** *Nature Reviews Drug Discovery* 2011**:**1-13.
623 37. Zoncu R, Efeyan A, Sabatini DM: **mTOR: from growth signal integration to cancer,**
624 **diabetes and ageing.** *Nature Reviews in Molecular Cell Biology* 2011, **12:**21-35.
625 38. Chi H: **Regulation and function of mTOR signalling in T cell fate decisions.** *Nature*
626 *Reviews Immunology* 2012**:**1-14.
627 39. Bischof E, Siow RC, Zhavoronkov A, Kaeberlein M: **The potential of rapalogs to**
628 **enhance resilience against SARS-CoV-2 infection and reduce the severity of COVID-**
629 **19.** *The Lancet Healthy longevity* 2021, **2:**e105-e111.
630 40. Kindrachuk J, Ork B, Hart BJ, Mazur S, Holbrook MR, Frieman MB, Traynor D, Johnson
631 RF, Dyall J, Kuhn JH, et al: **Antiviral potential of ERK/MAPK and PI3K/AKT/mTOR**
632 **signaling modulation for Middle East respiratory syndrome coronavirus infection as**
633 **identified by temporal kinome analysis.** *Antimicrobial Agents and Chemotherapy* 2015,
634 **59:**1088-1099.
635 41. Le Sage V, Cinti A, Amorim R, Mouland A: **Adapting the Stress Response: Viral**
636 **Subversion of the mTOR Signaling Pathway.** *Viruses* 2016, **8:**152-119.
637 42. Maiese K: **The Mechanistic Target of Rapamycin (mTOR): Novel Considerations as**
638 **an Antiviral Treatment.** *Current Neurovascular Research* 2020, **17:**332-337.
639 43. Buchkovich NJ, Yu Y, Zampieri CA, Alwine JC: **The TORrid affairs of viruses: effects**
640 **of mammalian DNA viruses on the PI3K-Akt-mTOR signalling pathway.** *Nature*
641 *Reviews Microbiology* 2008, **6:**266-275.

642 44. Alsuwaidi AR, George JA, Almarzooqi S, Hartwig SM, Varga SM, Souid A-K: **Sirolimus**
643 **alters lung pathology and viral load following influenza A virus infection.** *Respiratory*
644 *Research* 2017, **18:**136.
645 45. Huang C-T, Hung C-Y, Chen T-C, Lin C-Y, Lin Y-C, Chang C-S, He Y-C, Huang Y-L,
646 Dutta A: **Rapamycin adjuvant and exacerbation of severe influenza in an**
647 **experimental mouse model.** *Scientific Reports* 2017, **7:**873-878.
648 46. Shi G, Ozog S, Torbett BE, Compton AA: **mTOR inhibitors lower an intrinsic barrier**
649 **to virus infection mediated by IFITM3.** *Proceedings of the National Academy of*
650 *Sciences of the United States of America* 2018, **115:**E10069-E10078.
651 47. Shi G, Schwartz O, Compton AA: **More than meets the I: the diverse antiviral and**
652 **cellular functions of interferon-induced transmembrane proteins.** *Retrovirology* 2017,
653 **14:**1-11.
654 48. Perreira JM, Chin CR, Feeley EM, Brass AL: **IFITMs Restrict the Replication of**
655 **Multiple Pathogenic Viruses.** *Journal of Molecular Biology* 2013, **425:**4937-4955.
656 49. Rahman K, Coomer CA, Majdoul S, Ding SY, Padilla-Parra S, Compton AA: **Homology-**
657 **guided identification of a conserved motif linking the antiviral functions of IFITM3**
658 **to its oligomeric state.** *eLife* 2020, **9:**975-925.
659 50. Li K, Markosyan RM, Zheng Y-M, Golfetto O, Bungart B, Li M, Ding S, He Y, Liang C,
660 Lee JC, et al: **IFITM proteins restrict viral membrane hemifusion.** *PLoS Pathogens*
661 2013, **9:**e1003124.
662 51. Desai TM, Marin M, Chin CR, Savidis G, Brass AL, Melikyan GB: **IFITM3 restricts**
663 **influenza A virus entry by blocking the formation of fusion pores following virus-**
664 **endosome hemifusion.** *PLoS Pathogens* 2014, **10:**e1004048.
665 52. Lin T-Y, Chin CR, Everitt AR, Clare S, Perreira JM, Savidis G, Aker AM, John SP, Sarlah
666 D, Carreira EM, et al: **Amphotericin B Increases Influenza A Virus Infection by**
667 **Preventing IFITM3-Mediated Restriction.** *Cell Reports* 2013, **5:**895-908.
668 53. Guo X, Steinkühler J, Marin M, Li X, Lu W, Dimova R, Melikyan GB: **Interferon-**
669 **Induced Transmembrane Protein 3 Blocks Fusion of Diverse Enveloped Viruses by**
670 **Altering Mechanical Properties of Cell Membranes.** *ACS Nano* 2021.
671 54. Chesarino NM, Compton AA, McMichael TM, Kenney AD, Zhang L, Soewarna V, Davis
672 M, Schwartz O, Yount JS: **IFITM3 requires an amphipathic helix for antiviral activity.**
673 *EMBO Reports* 2017**:**e201744100-201744112.
674 55. Shi G, Kenney AD, Kudryashova E, Zani A, Zhang L, Lai KK, Hall-Stoodley L, Robinson
675 RT, Kudryashov DS, Compton AA, Yount JS: **Opposing activities of IFITM proteins in**
676 **SARS-CoV-2 infection.** *The EMBO Journal* 2020, **3:**e201900542-201900512.
677 56. Winstone H, Lista MJ, Reid AC, Bouton C, Pickering S, Galão RP, Kerridge C, Doores
678 KJ, Swanson C, Neil S: **The polybasic cleavage site in the SARS-CoV-2 spike**
679 **modulates viral sensitivity to Type I interferon and IFITM2.** *Journal of Virology* 202
680 57. Zhang Y, Qin L, Zhao Y, Zhang P, Xu B, Li K, Liang L, Zhang C, Dai Y, Feng Y, et al:
681 **Interferon-induced transmembrane protein-3 genetic variant rs12252-C is associated**
682 **with disease severity in COVID-19.** *The Journal of Infectious Diseases* 2020.
683 58. Nikoloudis D, Kountouras D, Hiona A: **The frequency of combined IFITM3 haplotype**
684 **involving the reference alleles of both rs12252 and rs34481144 is in line with COVID-**
685 **19 standardized mortality ratio of ethnic groups in England.** *PeerJ* 2020, **8:**e10402.
686 59. Bestle D, Heindl MR, Limburg H, Van Lam van T, Pilgram O, Moulton H, Stein DA,
687 Hardes K, Eickmann M, Dolnik O, et al: **TMPRSS2 and furin are both essential for**

688 **proteolytic activation of SARS-CoV-2 in human airway cells.** *Life Science Alliance*
689 2020, **3:**e202000786.
690 60. Hoffmann M, Kleine-Weber H, Pöhlmann S: **A Multibasic Cleavage Site in the Spike**
691 **Protein of SARS-CoV-2 Is Essential for Infection of Human Lung Cells.** *Molecular*
692 *Cell* 2020, **78:**779-784.e775.
693 61. Hoffmann M, Kleine-Weber H, Schroeder S, Krüger N, Herrler T, Erichsen S, Schiergens
694 TS, Herrler G, Wu N-H, Nitsche A, et al: **SARS-CoV-2 Cell Entry Depends on ACE2**
695 **and TMPRSS2 and Is Blocked by a Clinically Proven Protease Inhibitor.** *Cell* 2020**:**1-
696 19.
697 62. Park J-E, Li K, Barlan A, Fehr AR, Perlman S, McCray PB, Gallagher T: **Proteolytic**
698 **processing of Middle East respiratory syndrome coronavirus spikes expands virus**
699 **tropism.** *Proceedings of the National Academy of Sciences of the United States of America*
700 2016, **113:**12262-12267.
701 63. Shang J, Wan Y, Luo C, Ye G, Geng Q, Auerbach A, Li F: **Cell entry mechanisms of**
702 **SARS-CoV-2.** *Proceedings of the National Academy of Sciences* 2020, **117:**11727-11734.
703 64. Hou YJ, Okuda K, Edwards CE, Martinez DR, Asakura T, Kenneth H Dinnon, III, Kato T,
704 Lee RE, Yount BL, Mascenik TM, et al: **SARS-CoV-2 Reverse Genetics Reveals a**
705 **Variable Infection Gradient in the Respiratory Tract.** *Cell* 2020**:**1-83.
706 65. Fulcher ML, Randell SH: **Human nasal and tracheo-bronchial respiratory epithelial**
707 **cell culture.** *Methods in Molecular Biology* 2013, **945:**109-121.
708 66. Letko M, Marzi A, Munster V: **Functional assessment of cell entry and receptor usage**
709 **for SARS-CoV-2 and other lineage B betacoronaviruses.** *Nature Microbiology* 2020,
710 **11:**1-17.
711 67. Schuck S: **Microautophagy - distinct molecular mechanisms handle cargoes of many**
712 **sizes.** *Journal of Cell Science* 2020, **133**.
713 68. Mijaljica D, Prescott M, Devenish RJ: **Microautophagy in mammalian cells: revisiting**
714 **a 40-year-old conundrum.** *Autophagy* 2011, **7:**673-682.
715 69. Yang X, Zhang W, Wen X, Bulinski PJ, Chomchai DA, Arines FM, Liu Y-Y, Sprenger S,
716 Teis D, Klionsky DJ, Li M: **TORC1 regulates vacuole membrane composition through**
717 **ubiquitin- and ESCRT-dependent microautophagy.** *The Journal of Cell Biology* 2020,
718 **219**.
719 70. Li M, Rong Y, Chuang Y-S, Peng D, Emr SD: **Ubiquitin-Dependent Lysosomal**
720 **Membrane Protein Sorting and Degradation.** *Molecular Cell* 2015, **57:**467-478.
721 71. Chesarino NM, McMichael TM, Hach JC, Yount JS: **Phosphorylation of the antiviral**
722 **protein interferon-inducible transmembrane protein 3 (IFITM3) dually regulates its**
723 **endocytosis and ubiquitination.** *Journal of Biological Chemistry* 2014, **289:**11986-
724 11992.
725 72. Jia R, Xu F, Qian J, Yao Y, Miao C, Zheng Y-M, Liu S-L, Guo F, Geng Y, Qiao W, Liang
726 C: **Identification of an endocytic signal essential for the antiviral action of IFITM3.**
727 *Cellular Microbiology* 2014, **16**.
728 73. Jia R, Pan Q, Ding S, Rong L, Liu S-L, Geng Y, Qiao W, Liang C: **The N-terminal region**
729 **of IFITM3 modulates its antiviral activity by regulating IFITM3 cellular localization.**
730 *Journal of Virology* 2012, **86:**13697-13707.
731 74. Compton AA, Roy N, Porrot F, Billet A, Casartelli N, Yount JS, Liang C, Schwartz O:
732 **Natural mutations in IFITM3 modulate post-translational regulation and toggle**
733 **antiviral specificity.** *EMBO Reports* 2016, **17:**1657-1671.

734 75. Chesarino NM, McMichael TM, Yount JS: **Regulation of the trafficking and antiviral**
735 **activity of IFITM3 by post-translational modifications.** *Future Microbiology* 2014,
736 **9:**1151-1163.
737 76. Jia R, Ding S, Pan Q, Liu S-L, Qiao W, Liang C: **The C-Terminal Sequence of IFITM1**
738 **Regulates Its Anti-HIV-1 Activity.** *PLoS ONE* 2015, **10:**e0118794.
739 77. Li K, Jia R, Li M, Zheng YM, Miao C, Yao Y, Geng Y, Qiao W, Albritton LM, Liang C,
740 Liu SL: **A sorting signal suppresses ifitm1 restriction of viral entry.** *Journal of*
741 *Biological Chemistry* 2014, **290:**630780-634259.
742 78. Huang IC, Bailey CC, Weyer JL, Radoshitzky SR, Becker MM, Chiang JJ, Brass AL,
743 Ahmed AA, Chi X, Dong L, et al: **Distinct patterns of IFITM-mediated restriction of**
744 **filoviruses, SARS coronavirus, and influenza A virus.** *PLoS Pathogens* 2011,
745 **7:**e1001258.
746 79. Chesarino NM, McMichael TM, Yount JS: **E3 Ubiquitin Ligase NEDD4 Promotes**
747 **Influenza Virus Infection by Decreasing Levels of the Antiviral Protein IFITM3.** *PLoS*
748 *Pathogens* 2015, **11:**e1005095.
749 80. Kolos JM, Voll AM, Bauder M, Hausch F: **FKBP Ligands-Where We Are and Where**
750 **to Go?** *Frontiers in Pharmacology* 2018, **9:**1425.
751 81. Marz AM, Fabian AK, Kozany C, Bracher A, Hausch F: **Large FK506-Binding Proteins**
752 **Shape the Pharmacology of Rapamycin.** *Molecular and Cellular Biology* 2013, **33:**1357-
753 1367.
754 82. Hachim MY, Al Heialy S, Hachim IY, Halwani R, Senok AC, Maghazachi AA, Hamid Q:
755 **Interferon-Induced Transmembrane Protein (IFITM3) Is Upregulated Explicitly in**
756 **SARS-CoV-2 Infected Lung Epithelial Cells.** *Frontiers in Immunology* 2020, **11:**1372.
757 83. Blanco-Melo D, Nilsson-Payant BE, Liu W-C, Uhl S, Hoagland D, Møller R, Jordan TX,
758 Oishi K, Panis M, Sachs D, et al: **Imbalanced Host Response to SARS-CoV-2 Drives**
759 **Development of COVID-19.** *Cell* 2020, **181:**1036-1045.e1039.
760 84. Sungnak W, Huang N, Bécavin C, Berg M, Queen R, Litvinukova M, Talavera-López C,
761 Maatz H, Reichart D, Sampaziotis F, et al: **SARS-CoV-2 entry factors are highly**
762 **expressed in nasal epithelial cells together with innate immune genes.** *Nature Medicine*
763 2020, **26:**1-14.
764 85. Ziegler CGK, Miao VN, Owings AH, Navia AW, Tang Y, Bromley JD, Lotfy P, Sloan M,
765 Laird H, Williams HB, et al: **Impaired local intrinsic immunity to SARS-CoV-2**
766 **infection in severe COVID-19.** *bioRxiv* 2021**:**2021.2002.2020.431155.
767 86. Chiramel AI, Meyerson NR, McNally KL, Broeckel RM, Montoya VR, Méndez-Solís O,
768 Robertson SJ, Sturdevant GL, Lubick KJ, Nair V, et al: **TRIM5α Restricts Flavivirus**
769 **Replication by Targeting the Viral Protease for Proteasomal Degradation.** *Cell*
770 *Reports* 2019, **27:**3269-3283.e3266.
771 87. Compton AA, Bruel T, Porrot F, Mallet A, Sachse M, Euvrard M, Liang C, Casartelli N,
772 Schwartz O: **IFITM Proteins Incorporated into HIV-1 Virions Impair Viral Fusion**
773 **and Spread.** *Cell Host & Microbe* 2014, **16:**736-747.
774

775
776
777
778

Figures and Figure Captions

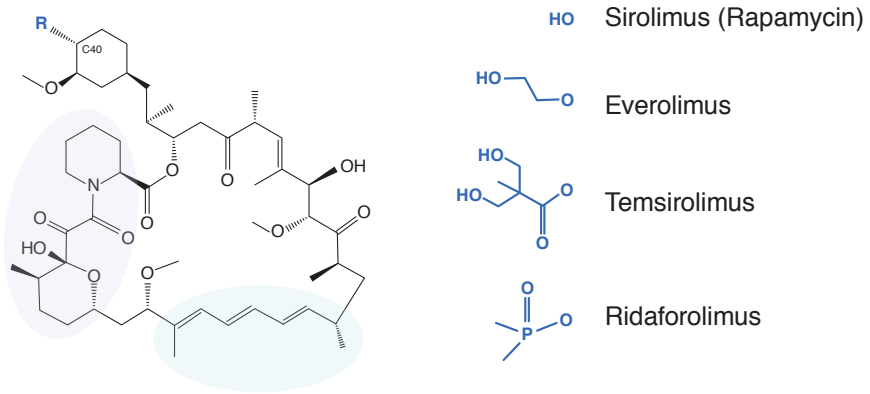

Figure 1: Rapamycin analogs share the same macrolide structure but differ by the functional group present at carbon-40. Violet and green bubbles indicate the FKBP12- and mTOR-binding sites, respectively.

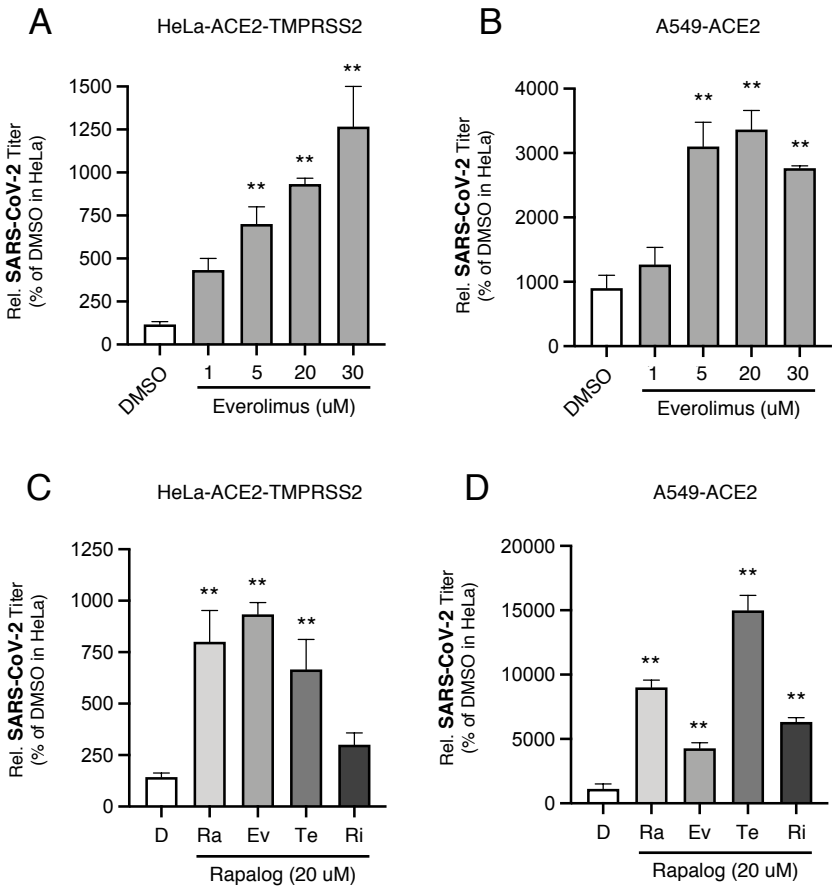

Figure 2: Rapalogs promote SARS-CoV-2 infection in cervical and lung epithelial cell lines in a dose-dependent and drug-dependent manner.

(A) HeLa-ACE2-TMPRSS2 cells were treated with increasing concentrations of everolimus for 4 hours and subsequently exposed to SARS-CoV-2 at an MOI of 0.1. A volume of DMSO corresponding to the highest dose of everolimus served as vehicle control. Virus-containing supernatants were harvested at 24 hours and titered on Vero E6 cells by plaque assay and plaque-forming units (pfu) per mL was normalized to 100 in the DMSO condition. (B) A549-ACE2 cells were treated as in (A) and pfu per mL was normalized to the DMSO condition in HeLa-ACE2-TMPRSS2 cells. (C) HeLa-ACE2-TMPRSS2 cells were treated with 20 µM of rapamycin (Ra), everolimus (Ev), temsirolimus (Te), ridaforolimus (Ri), or an equivalent volume of DMSO (D) for 4 hours and subsequently exposed to SARS-CoV-2 at an MOI of 0.1. Virus-containing supernatants were harvested at 24 hours and titered on Vero E6 cells by plaque assay and pfu per mL was normalized to 100 in the DMSO condition. (D) A549-ACE2 cells were treated as in (C) and pfu per mL was normalized to the DMSO condition in HeLa-ACE2-TMPRSS2 cells. All error bars represent standard error calculated from 3-5 experiments. Statistical analysis was performed with one-way ANOVA and asterisks indicate significant difference from DMSO. *, $p < 0.05$; **, $p < 0.01$.

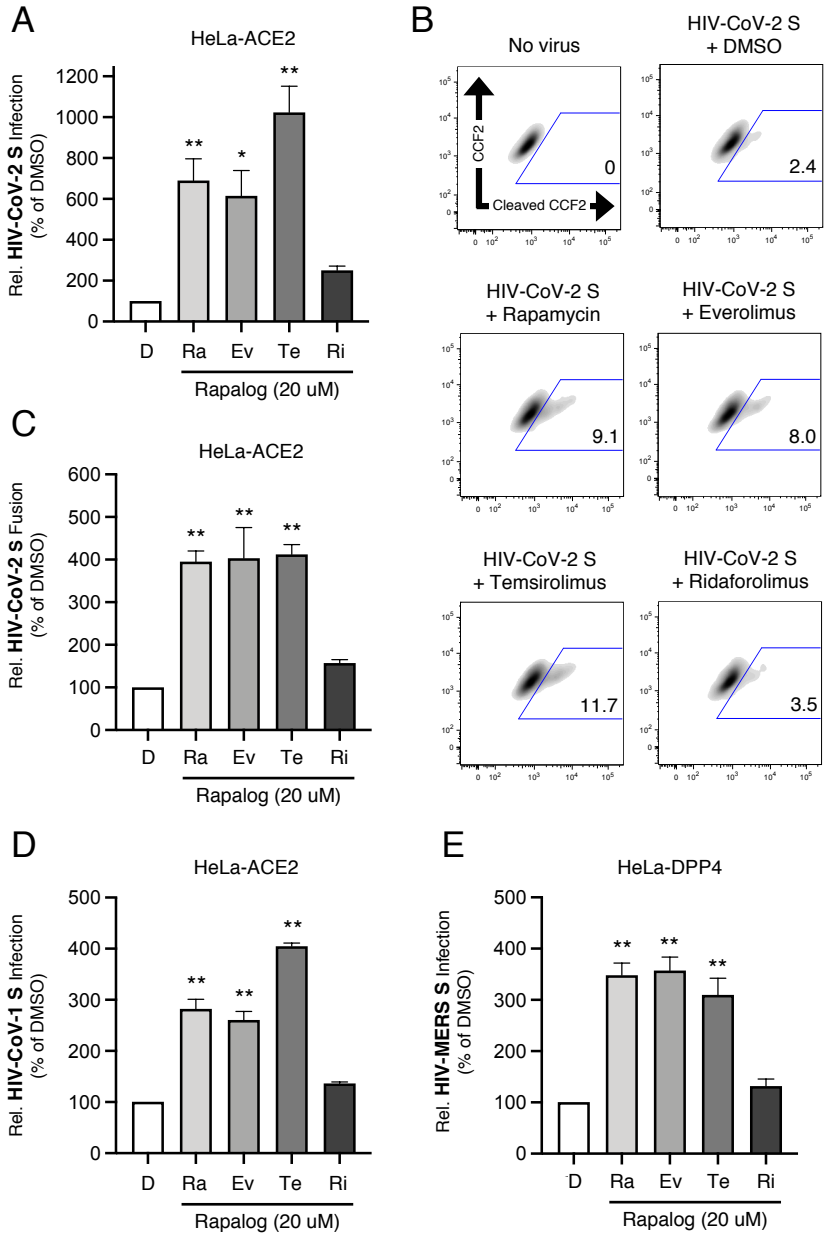

Figure 3: Rapalogs boost the cell entry step of infection mediated by Spike proteins from SARS-CoV-2, SARS-CoV, and MERS.

(A) HeLa-ACE2 cells were treated with 20 µM of rapamycin (Ra), everolimus (Ev), temsirolimus (Te), ridaforolimus (Ri), or an equivalent volume of DMSO (D) for 4 hours and subsequently exposed to HIV-CoV-2 S pseudovirus. Cells were lysed at 48 hours and luciferase activity was measured. Luciferase units were normalized to 100 in the DMSO condition. (B) HeLa-ACE2 cells were treated with 20 µM of rapamycin (Ra), everolimus (Ev), temsirolimus (Te), ridaforolimus (Ri), or an equivalent volume of DMSO (D) for 4 hours and subsequently exposed to HIV-CoV-2 S pseudovirus incorporating BlaM-Vpr for 2 hours. Cells were incubated with CCF2-AM for an additional 2 hours and fixed. Cleaved CCF2 was measured by flow cytometry. Dot plots visualized as density plots from one representative experiment are shown and the percentage of CCF2+ cells

823 which exhibit CCF2 cleavage is indicated. (C) Summary data for (B) representing the average of
824 three experiments. (D) As in (A), except cells were exposed to HIV-CoV S pseudovirus. (E) As in
825 (A), except HeLa-DPP4 cells were exposed to HIV-MERS S pseudovirus. All error bars represent
826 standard error calculated from 3-4 experiments. Statistical analysis was performed with one-way
827 ANOVA and asterisks indicate significant difference from DMSO. *, $p < 0.05$; **, $p < 0.01$.
828
829
830
831
832
833
834
835
836
837
838
839
840
841
842
843
844
845
846
847
848
849
850
851
852
853

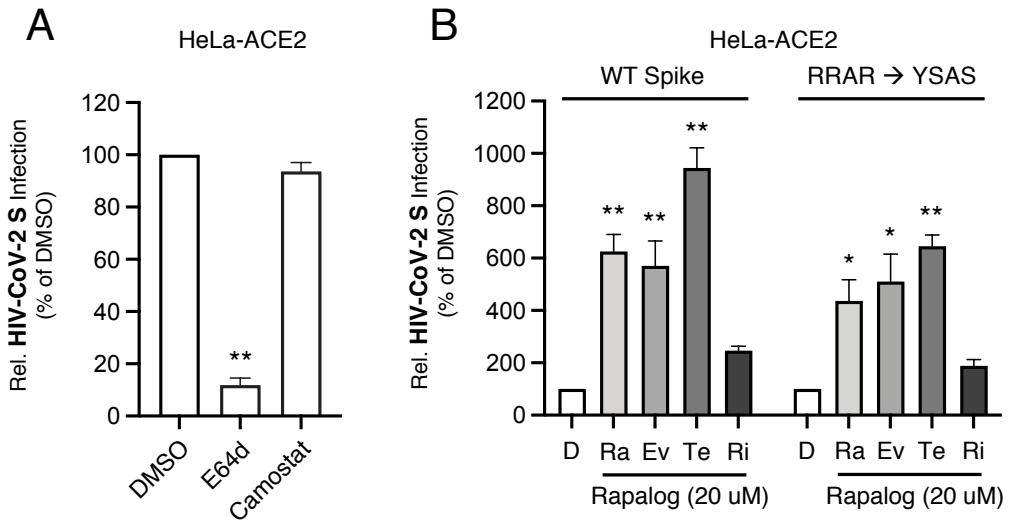

Figure 4: Rapalogs facilitate endocytic entry of HIV-CoV-2 S pseudovirus into HeLa-ACE2 cells.

(A) HeLa-ACE2 cells were treated with 25 μM of E64d, camostat mesylate, or an equivalent volume of DMSO for 2 hours and subsequently exposed to HIV-CoV-2 S pseudovirus. At 48 hours, cells were lysed and luciferase activity was measured. Luciferase units were normalized to 100 in the DMSO condition. (B) HeLa-ACE2 cells were treated with 20 μM of rapamycin (Ra), everolimus (Ev), temsirolimus (Te), ridaforolimus (Ri), or an equivalent volume of DMSO (D) for 4 hours and subsequently exposed to HIV-CoV-2 S pseudovirus bearing WT or $_{682}$YSAS$_{685}$ Spike. Cells were lysed at 48 hours and luciferase activity was measured. Luciferase units were normalized to 100 in the DMSO condition. All error bars represent standard error calculated from 3 experiments. Statistical analysis was performed with one-way ANOVA and asterisks indicate significant difference from DMSO. *, $p < 0.05$; **, $p < 0.01$.

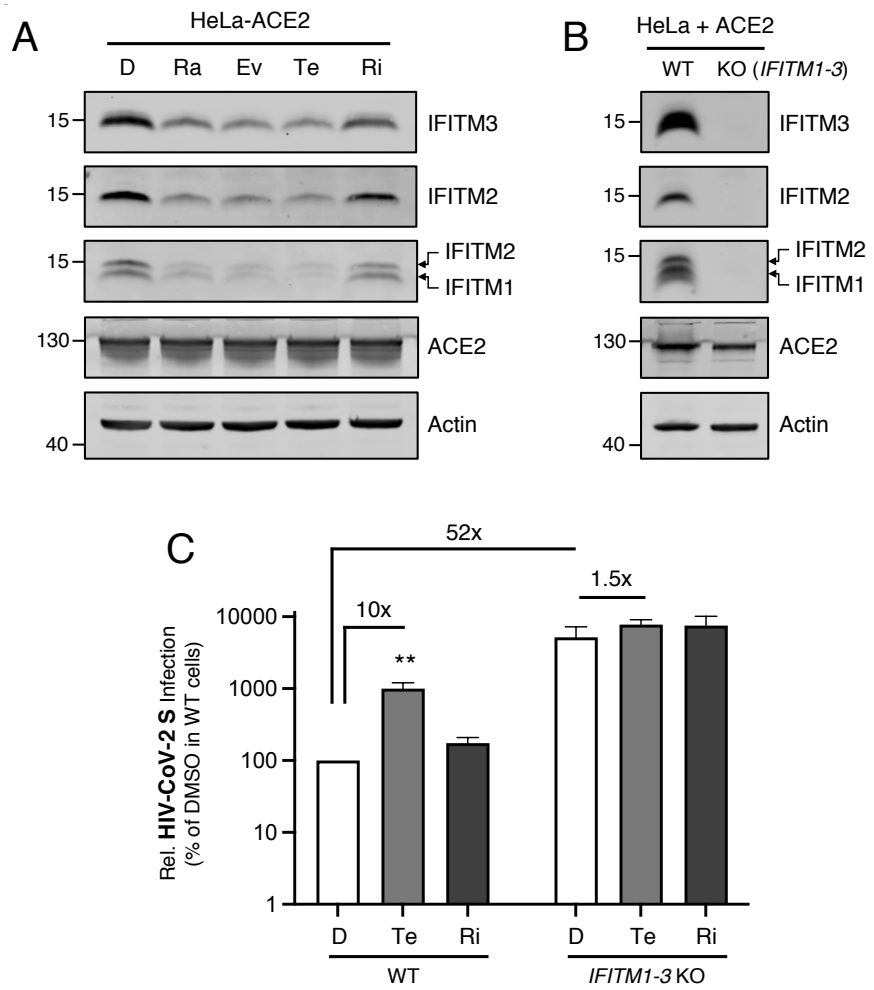

Figure 5: Human IFITM proteins restrict Spike-mediated infection and their levels are decreased differentially by rapalogs.

(A) HeLa-ACE2 cells were treated with 20 µM of rapamycin (Ra), everolimus (Ev), temsirolimus (Te), ridaforolimus (Ri), or an equivalent volume of DMSO (D) for 4 hours and whole cell lysates were subjected to SDS-PAGE and Western blot analysis. Immunoblotting was performed with anti-IFITM2, anti-IFITM3, anti-IFITM1, anti-ACE2, and anti-actin (in that order) on the same nitrocellulose membrane. (B) Whole cell lysates from HeLa and HeLa *IFITM1-3* KO cells transiently transfected with ACE2 were subjected to SDS-PAGE and Western blot analysis. Immunoblotting was performed with anti-IFITM2, anti-IFITM3, anti-IFITM1, anti-ACE2, and anti-actin (in that order) on the same nitrocellulose membrane. Numbers and tick marks indicate size (kilodaltons) and position of protein standards in ladder. (C) HeLa and HeLa *IFITM1-3* KO cells were transiently transfected with ACE2 for 24 hours and subsequently treated with 20 µM of temsirolimus (Te), ridaforolimus (Ri), or an equivalent volume of DMSO (D) for 4 hours. Cells were exposed to HIV-CoV-2 S pseudovirus and luciferase activity was measured 48 hours later. Luciferase units were normalized to 100 in the DMSO condition of WT cells. All error bars represent standard error calculated from 4 experiments. Statistical analysis was performed with one-way ANOVA and asterisks indicate significant difference from DMSO. *, $p < 0.05$; **, $p < 0.01$.

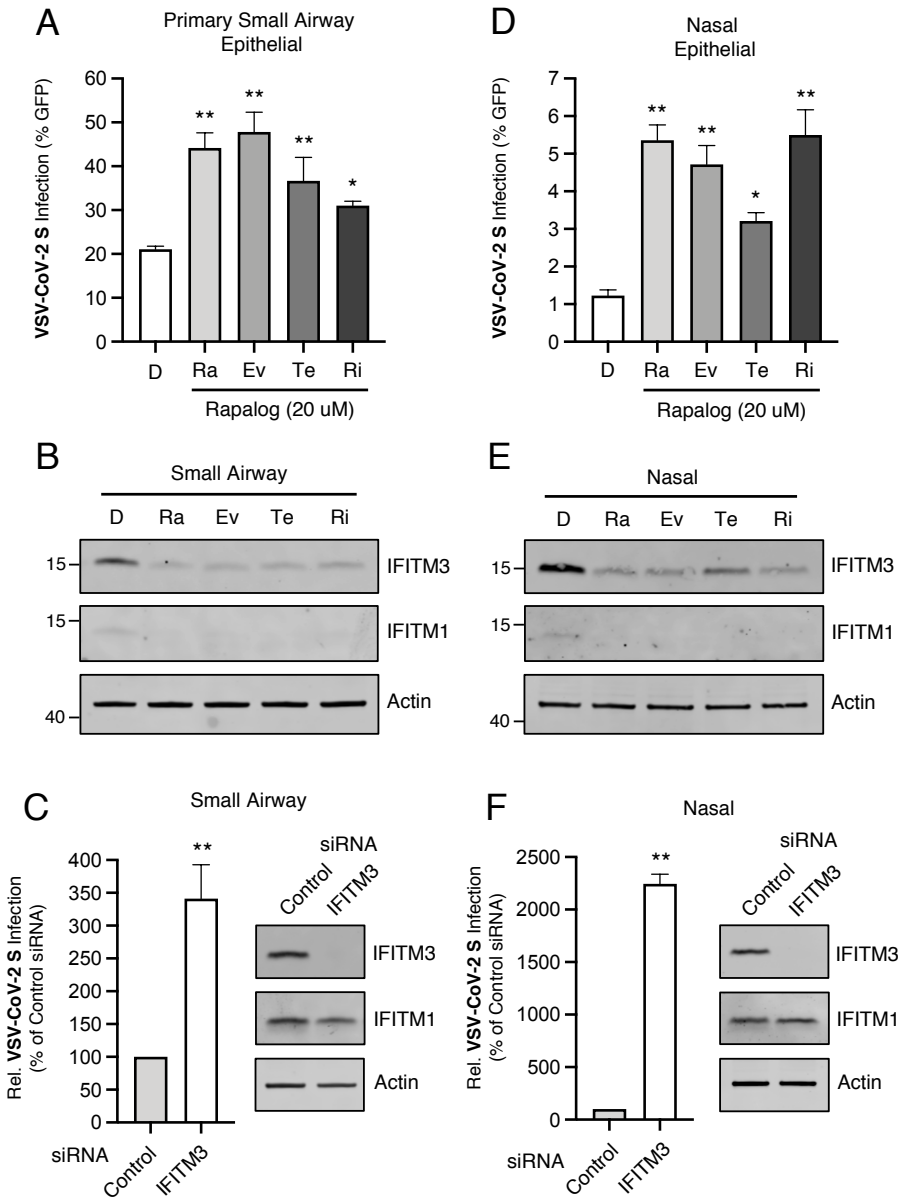

Figure 6: Rapalogs promote infection mediated by SARS-CoV-2 Spike in primary lung and nasal cells.

(A) Primary human small airway epithelial cells were treated with 20 μM of rapamycin (Ra), everolimus (Ev), temsirolimus (Te), ridaforolimus (Ri), or an equivalent volume of DMSO (D) for 4 hours and subsequently exposed to VSV-CoV-2 S pseudovirus. Cells were fixed at 24 hours and infection was scored by measuring GFP+ cells with flow cytometry. (B) Whole cell lysates from primary small airway epithelial cells were subjected to SDS-PAGE and Western blot analysis. Immunoblotting was performed with anti-IFITM2, anti-IFITM3, anti-IFITM1, and anti-actin (in that order) on the same nitrocellulose membrane. (C) Primary human small airway epithelial cells were transfected with siRNA targeting IFITM3 or a non-targeting control siRNA and exposed to VSV-CoV-2 S pseudovirus 48 hours later. At 24 hours post-virus addition, cells were lysed and luciferase activity was measured. Luciferase units were normalized to 100 in the control siRNA condition. siRNA-transfected cells were subjected to SDS-PAGE and Western blot analysis with

anti-IFITM2, anti-IFITM3, anti-IFITM1, and anti-actin (in that order) on the same nitrocellulose membrane. (D) Semi-transformed human nasal epithelial cells were treated with 20 μM of rapamycin (Ra), everolimus (Ev), temsirolimus (Te), ridaforolimus (Ri), or an equivalent volume of DMSO (D) for 4 hours and subsequently exposed to VSV-CoV-2 S pseudovirus. Cells were fixed at 24 hours and infection was scored by measuring GFP+ cells with flow cytometry. (E) Whole cell lysates from human nasal epithelial cells were subjected to SDS-PAGE and Western blot analysis. Immunoblotting was performed with anti-IFITM2, anti-IFITM3, anti-IFITM1, and anti-actin (in that order) on the same nitrocellulose membrane. (F) Human nasal epithelial cells were transfected with 20 nM siRNA targeting IFITM3 or a non-targeting control siRNA and exposed to VSV-CoV-2 S pseudovirus 48 hours later. At 24 hours post-virus addition, cells were lysed and luciferase activity was measured. Luciferase units were normalized to 100 in the control siRNA condition. siRNA-transfected cells were subjected to SDS-PAGE and Western blot analysis with anti-IFITM2, anti-IFITM3, anti-IFITM1, and anti-actin (in that order) on the same nitrocellulose membrane. Numbers and tick marks indicate size (kilodaltons) and position of protein standards in ladder. All error bars represent standard error calculated from 3-4 experiments. Statistical analysis in (A) and (D) was performed with one-way ANOVA and asterisks indicate significant difference from DMSO. Statistical analysis in (C) and (F) was performed with Student's T test and asterisks indicate significant difference from control siRNA. *, $p < 0.05$; **, $p < 0.01$.

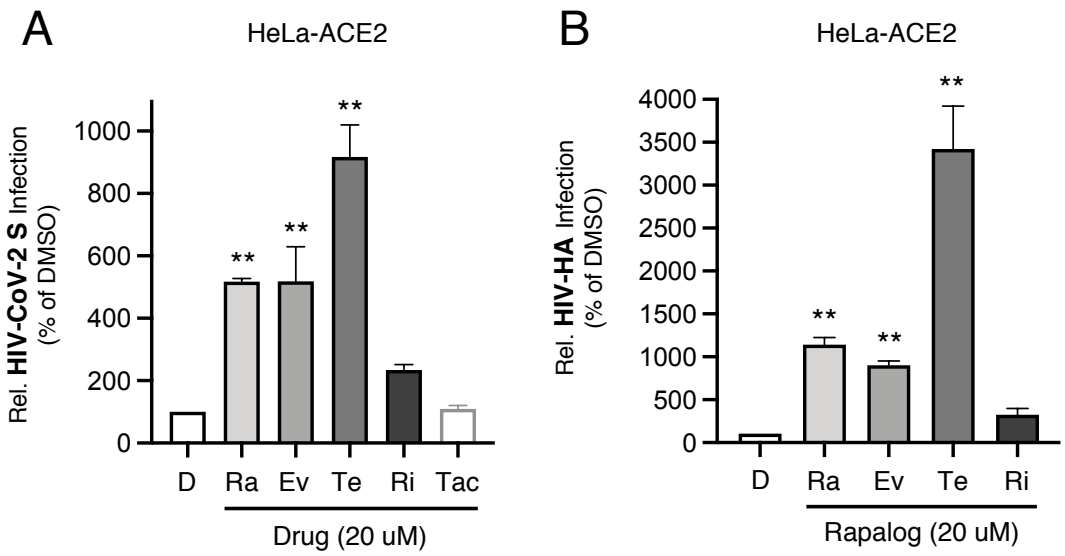

Supplemental Figure 1:
(A) HeLa-ACE2 cells were treated with 20 μM of rapamycin (Ra), everolimus (Ev), temsirolimus (Te), ridaforolimus (Ri), tacrolimus (Tac), or an equivalent volume of DMSO (D) for 4 hours and subsequently exposed to HIV-CoV-2 S pseudovirus. Cells were lysed at 48 hours and luciferase activity was measured. Luciferase units were normalized to 100 in the DMSO condition. (B) HeLa-ACE2 cells were treated with 20 μM of rapamycin (Ra), everolimus (Ev), temsirolimus (Te), ridaforolimus (Ri), or an equivalent volume of DMSO (D) for 4 hours and subsequently exposed to HIV-HA pseudovirus. Cells were lysed at 48 hours and luciferase activity was measured. Luciferase units were normalized to 100 in the DMSO condition. All error bars represent standard error calculated from 3 experiments. Statistical analysis was performed with one-way ANOVA and asterisks indicate significant difference from DMSO. *, $p < 0.05$; **, $p < 0.01$.

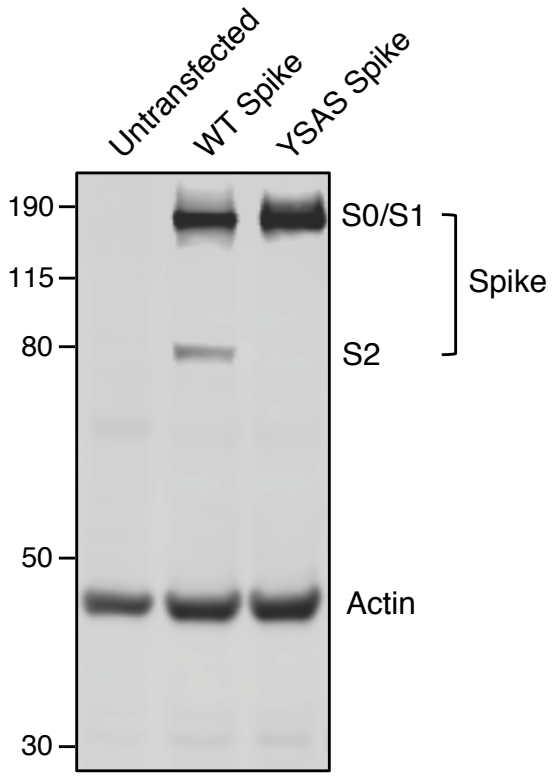

949
950 **Supplemental Figure 2:**
951 HEK293T cells were transfected with pcDNA3.1 encoding WT SARS-CoV-2 Spike or Spike
952 encoding $_{682}$YSAS$_{685}$ for 48 hours and subsequently subjected to SDS-PAGE and Western blot
953 analysis. Immunoblotting was performed with anti-Spike and anti-actin. Numbers and tick marks
954 indicate size (kilodaltons) and position of protein standards in ladder.
955
956
957
958
959
960
961
962
963
964
965

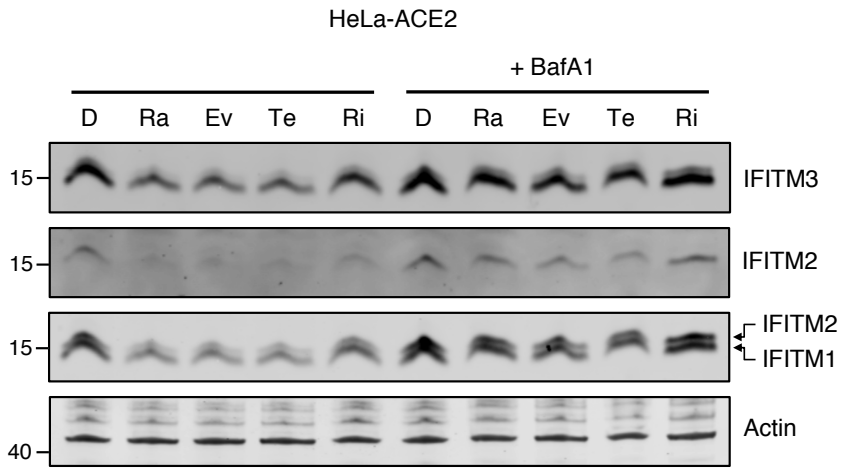

Supplemental Figure 3:
HeLa-ACE2 cells were treated with 20 µM of rapamycin (Ra), everolimus (Ev), temsirolimus (Te), ridaforolimus (Ri), or an equivalent volume of DMSO (D), in the absence or presence of 1 µM bafilomycin A1, for 4 hours. Whole cell lysates were subjected to SDS-PAGE and Western blot analysis with anti-IFITM2, anti-IFITM3, anti-IFITM1, and anti-actin (in that order) on the same nitrocellulose membrane.

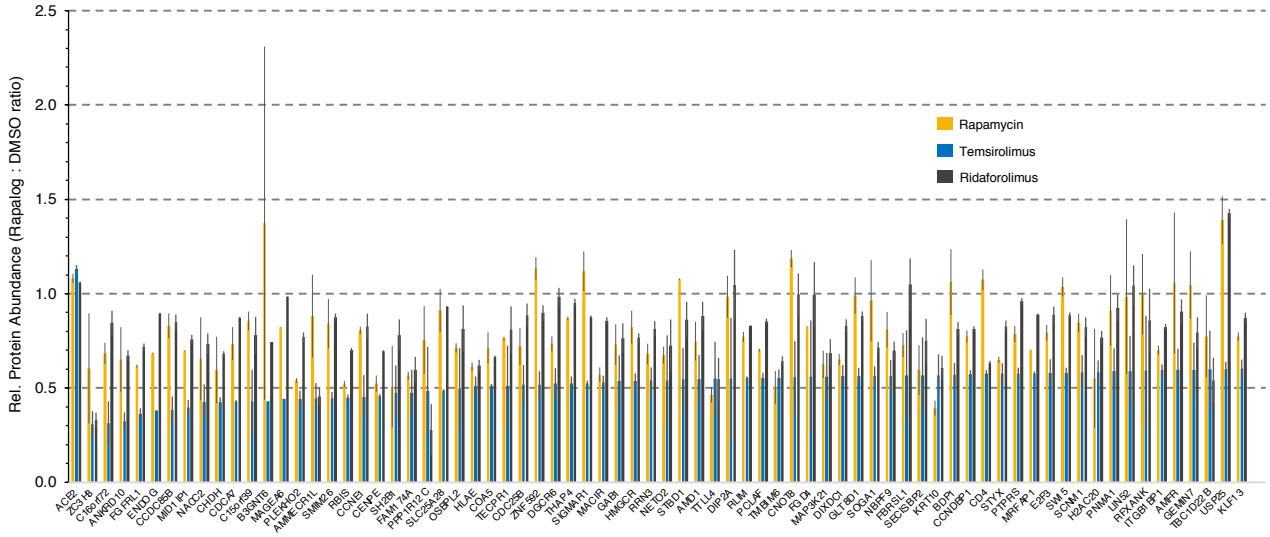

Supplemental Figure 4:
HeLa-ACE2 cells were treated with 20 µM of rapamycin, temsirolimus, ridaforolimus, or an equivalent volume of DMSO for 4 hours and proteins were extracted for analysis by mass spectrometry. 7023 proteins were detected in all conditions and the raw data is presented in Supplemental File 1. The 73 proteins which exhibited a temsirolimus to DMSO ratio of 0.60 or less are shown. ACE2 is also shown for comparison.

Supplemental File 1: Spreadsheet of proteomics data obtained by mass spectrometry.